JPE 17-2-12

https://doi.org/10.6113/JPE.2017.17.2.432
ISSN(Print): 1598-2092 / ISSN(Online): 2093-4718

BPF-based Grid Voltage Feedforward Control of Grid-connected Converters for Improving Robust Stability

Shude Yang†, Xiangqian Tong*,**, Jun Yin*, Haiyan Wang*, Yaping Deng*, and Le Liu*

†,*School of Automation and Information Engineering, Xi'an University of Technology, Xi'an, China
**Xi'an Hailian Petrochemical Technologies Co., Ltd., Xi'an, China

Abstract

Grid voltage feedforward is extensively used for controlling grid-connected converters. However, the conventional voltage feedforward control reduces the stability margins of the converter connected to a high-impedance grid. The effect mechanism of voltage feedforward on the grid-connected converter control under high-inductive conditions of the grid impedance is clearly explained in this study using the equivalent transformations of control block diagrams. Results show that the delay produced by the digital control is the root cause of this effect. An improved voltage feedforward strategy, in which a bandpass filter (BPF) is introduced into the feedforward path, is proposed to strengthen the converter's robust stability against grid impedance variations. The selection method of the BPF's bandwidth is also provided considering the tradeoff between the response speed to the grid voltage sag and the system's robust stability. The converter can work stably over a wide range of the grid impedance through the proposed approach. Simulation and experimental results fully verify the effectiveness of the BPF-based voltage feedforward strategy.

Key words: Bandpass filter, Delay caused by digital control, Grid-connected converter, Grid impedance, Grid voltage feedforward, Robust stability

I. INTRODUCTION

Recently, grid-connected converters are considered a key enabling technology to realize distributed generation (solar and wind) interfaces [1], [2], static var generator [3], and active power filters [4]. With the continuous spread of these devices, multiple low-power transformers and long transmission lines are used to connect these devices to the public grid because of the scattered locations of the distributed generation and nonlinear loads. Therefore, grid impedance may vary over a wide range [5]. Moreover, the regulation for optimizing power system operation may change the grid configuration periodically; this process affects the grid impedance remarkably even at the same point of common coupling (PCC) [6]. Furthermore, other factors, such as the faults, tripping of lines and load variations, can cause grid impedance variations. A grid may have large inductive impedance suffering from these parameter variations, which challenges system stability [7]. Simultaneously, given the standard for the distributed resources with electric power systems, a grid-connected converter should be operated stably under short circuit ratio (SCR)>20 [8], and the similar standard in China follows SCR>10 [9]. Therefore, the control system of the grid-connected converter should be designed with strong robust stability against grid impedance variations.

High-order filters can effectively attenuate the harmonics with less weight and volume; thus, this solution has become the preference for a grid-connected converter, such as the LCL, LLCL, or LTCL filter [10]-[12]. However, the time-varying inductive grid impedance will cause the variations in the resonance frequency of the high-order filter, which may compromise system stability [5], and this situation will be aggravated by the increasing connection of the grid converters in parallel [13], [14]. To overcome these drawbacks, [15] and

Manuscript received Jul. 31, 2016; accepted Jan. 20, 2017
Recommended for publication by Associate Editor Se-Kyo Chung.
†Corresponding Author: yangshude858755@163.com
Tel: +86-029-82312002, Xi'an University of Technology
*School of Automation & Information Eng., Xi'an Univ. of Tech., China
**Xi'an Hailian Petrochemical Technologies Co., Ltd., China

[16] proposed an online grid impedance estimation method to compensate for the resonance frequency of the LCL and LLCL filters, respectively. Furthermore, several other researchers have been interested in improving the robust stability of grid-connected converters with a high-order filter to overcome large grid inductance variations [17]-[20].

The phase-locked loop (PLL) of the synchronous reference frame is widely applied in grid-connected converter control. However, under high grid impedance conditions, the converter may also suffer from instability due to the interaction dynamics between grid impedance and PLL [21]. A high bandwidth PLL contributes to the increase of the negative real part of the converter output impedance, which challenges system damping [22]. Therefore, [23] suggested a significant reduction of the PLL gains to avoid instabilities. Moreover, PLL-less controllers have been recently developed (e.g., [24], [25]). Hence, the necessity for the PLL is eliminated, and an effective control performance was yielded under high grid impedance conditions.

In addition to the aforementioned reasons, the feedforward control for the grid voltage, which is widely used for improving the startup performance of grid-connected converters [26], can also result in instability when the grid has large inductive impedance [27]. However, limited literature discussed the control system performance with the voltage feedforward under this condition. In [28], an adaptive voltage feedforward control strategy has been implemented for single-phase grid-connected converters to improve its robust stability against grid impedance variations. However, the strategy depends on the online estimation of the grid impedance to ensure a satisfactory performance, which increases the complexity of the control system.

The search for a simple voltage feedforward strategy of a good industrial applicability and robust stability is still an arduous task. The *L*-filtered converter is considered the research plant in the following study for a concise and clear analysis of this problem, considering that the instability problem caused by the grid voltage feedforward exists for both *L*- and *LCL*-filtered converter. In this study, the effect mechanism of the voltage feedforward on the control system is clearly explained. A fundamental voltage feedforward method is proposed to improve the converter's robust stability against the wide-range variation of inductive grid impedance; this method only requires incorporating a bandpass filter (BPF) in the feedforward path.

This paper is organized as follows. In Section II, the mathematical model of the *L*-filtered grid-connected converter with voltage feedforward control is derived considering the grid impedance. Afterward, the effect mechanism of the voltage feedforward on the control system is revealed through equivalent transformations of control block diagrams. The converter's robust stability with the conventional voltage feedforward control is investigated in Section III. A BPF-based grid voltage feedforward method for improving the converter's robust stability against grid impedance variation is proposed in Section IV, and the impact of the BPF's bandwidth on the converter's robust stability is also analyzed. A theoretical analysis and the effectiveness of the proposed BPF-based voltage feedforward method are verified by the simulation and experimental results in Section V. Finally, Section VI concludes this paper.

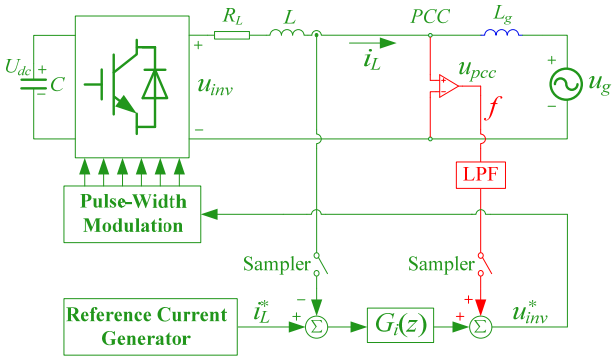

Fig. 1. Topology and current control architecture of the *L*-filtered grid-connected converter with voltage feedforward.

II. System Modeling and Analysis of the Effect Mechanism of the Grid Voltage Feedforward on the Control System

A. Modeling of the System with Voltage Feedforward Control Considering Grid Impedance

Fig. 1 shows the topology and control diagram of a digitally controlled grid-connected converter with an *L*-filter, where u_{inv} is the converter output voltage at the AC side, R_L is the equivalent series resistance of the *L*-filter, and u_g is the grid voltage.

The grid current i_L is regulated by the current regulator $G_i(z)$, which can be a proportional–integral, proportional–resonant, or repetitive controller (RC). The reference i_L^* includes the active current for the DC voltage control and the other components, which can be determined by an online calculation or manual setting. For voltage feedforward control, the voltage at the PCC denoted by u_{pcc} is sampled after filtration by the low-pass filter (LPF); then, this voltage is directly added into the output of the current regulator. Generally, the grid impedance at the PCC consists of inductance and resistance. Pure inductance L_g is considered in this process to draw the worst case, considering that grid resistance offers some degree of damping and helps in stabilizing the system. The relation between u_{pcc} and u_g in Fig. 1 can be explained by:

$$u_{pcc}(s) = L_g s \cdot i_L(s) + u_g(s) . \tag{1}$$

For a digitally controlled system of the converter, the pulse-width modulation (PWM) reference is commonly calculated in the current sampling period. However, PWM reference is updated until the next sampling time step

(namely, the "one-step-delay" control mode in digital control) to avoid incomplete control actions. Therefore, computation delay occurs. The s-domain can be expressed as $e^{-T_s s}$, where T_s is the sampling period. The zero-order hold (i.e., $(1-e^{-T_s s})/s$) is usually used to represent the modulation delay, because the PWM reference remains constant during one sampling period. Furthermore, the sampler is usually modeled as $1/T_s$ [13]. Given these delay factors and Eq. (1), the digitally controlled grid-connected converter, together with its control structure shown in Fig. 1, can be modeled as Fig. 2, where $G_g(s)$ is the grid impedance, $G_d(s)$ represents the delays produced by the digital control, $G_P(s)$ is the controlled plant, and $G_F(s)$ is the LPF in the feedforward path used for voltage filtering. They can be expressed as

$$G_g(s) = L_g s, \tag{2}$$

$$G_d(s) = \frac{1}{T_s}\cdot e^{-T_s s}\cdot\frac{1-e^{-T_s s}}{s} \approx e^{-1.5T_s s} \approx \frac{1-0.75T_s s}{1+0.75T_s s}, \tag{3}$$

$$G_P(s) = \frac{1}{(L+L_g)s + R_L}, \tag{4}$$

and

$$G_F(s) = \frac{1}{\frac{1}{\omega_c^2}s^2 + \frac{1}{Q\omega_c}s + 1} \tag{5}$$

where ω_c and Q are the cutoff frequency and quality factor of the LPF, correspondingly.

$D(s)=1-G_F(s)G_d(s)$ and $G_L(s)=1/(R_L+Ls)$ are defined to simplify the following expression. Then, according to Fig. 2, the error transfer function of the control system with the voltage feedforward can be obtained by

$$E(s) = \frac{i_L^*[1+G_L(s)G_g(s)D(s)] + G_L(s)D(s)u_g(s)}{1+G_i(s)G_d(s)G_L(s)+G_L(s)G_g(s)D(s)}. \tag{6}$$

This equation is used to analyze the converter's robust stability in this study.

B. Analysis of the Effect Mechanism of the Voltage Feedforward on the Control System

If the grid voltage feedforward is unused (i.e., the path denoted by f in Fig. 1 is removed), then the control diagram of the grid-side current without voltage feedforward can be obtained, as shown in Fig. 3. When the voltage feedforward is not adopted, the variations of the inductive grid impedance can be equivalent to the inductance variations of the L-filter, considering the equation $G_p(s)=1/[(L+L_g)s+R_L]$. This variation may cause current oscillation [29]. Hence, the converter's robust stability against grid impedance variations will also be affected even though the voltage feedforward is not adopted.

When the voltage feedforward control is adopted, as shown in Fig. 2, the feedforward path brings an additional positive feedback loop of i_L due to the existing grid impedance; this

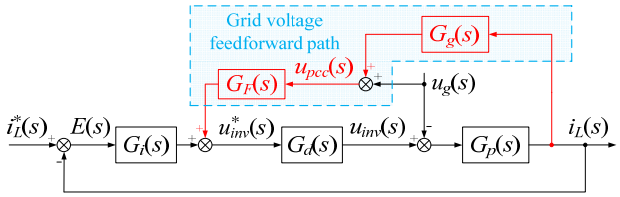

Fig. 2. Linearized average model of the grid-connected converter with voltage feedforward control.

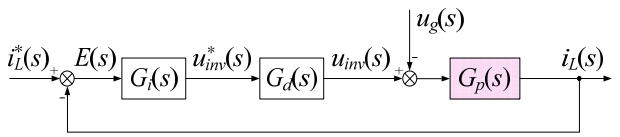

Fig. 3. Control diagram of the grid-side current without voltage feedforward control.

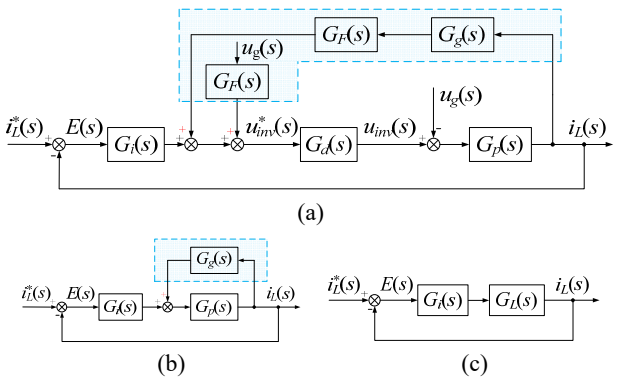

Fig. 4. Control diagram of the grid-connected converter. (a) Equivalent transformation of Fig. 2. (b) Equivalent diagram of Fig. 4(a) with $G_d(s)=G_F(s)=1$. (c) Simplified block diagram of Fig. 4(b).

dynamic interaction between the feedforward voltage and the grid-side current changes the control structure, which may affect system performance. Therefore, studying the mechanism of this effect is crucial, because this mechanism may provide a solution to the problem.

In Fig. 2, a series of equivalent transformations can be fulfilled; these transformations are shown in Fig. 4. First, the equivalent block diagram (Fig. 4(a)) can be obtained by decomposing the feedforward voltage u_{pcc} in Fig. 2 into the ideal grid voltage u_g and the voltage drop across the grid impedance. Second, assuming that delays do not occur in the voltage filtering and digital control (i.e., $G_d(s)=G_F(s)=1$), Fig. 4(a) can be equivalently transformed into Fig. 4(b). Third, the relations among $G_L(s)$, $G_g(s)$, and $G_P(s)$ in Eqs. (2) and (4) can be derived as $G_L(s)=G_P(s)/[1-G_P(s)G_g(s)]$. Thus, the simplified block diagram of Fig. 4(b) can be obtained (Fig. 4(c)). This diagram shows that if the delays in the voltage filtering and digital control can be eliminated, then the equivalent controlled plant is only related to the nominal value of the L-filter. Thus, when grid impedance varies, the system's robust stability remains unaffected. The converter's robust stability is improved compared with the control system without voltage

feedforward, as shown in Fig. 3.

Thus, if delays do not occur in the voltage filtering and digital control, then the interaction between the feedforward voltage and the grid-side current is conducive to the converter's robust stability against grid impedance variations. Therefore, the root cause of the effect of the voltage feedforward on the control system is the delay in the feedforward path. This delay can be produced by the LPF used for voltage filtering and digital control. However, these delays cannot be eliminated due to the feature of the digitally controlled system. Therefore, the voltage feedforward will inevitably affect the characteristics of the control system. The manner in which the voltage feedforward affects the converter's robust stability is analyzed in the next section.

III. Robust Stability Analysis of the Conventional Grid Voltage Feedforward Method

The converter's robust stability with the conventional voltage feedforward control is specifically analyzed in this section. The grid voltage at the PCC usually contains various background harmonics due to the large inductive impedance, which can be caused by the nonlinear load current flowing through the grid impedance. These harmonics can significantly distort the injected grid current, resulting in poor power quality. Therefore, the RC is applied in this study for high-harmonic rejection capability to improve the quality of the grid-side current [30]. In addition, the proportional gain is paralleled with the RC to improve the transient response. The structure of the entire current regulator is depicted in Fig. 5 where $E(z)$ is the tracking error; k_p is the proportional gain; $q(z)$ is the stabilization filter, which can be a constant close to 1 or an LPF; N is the number of samples in one fundamental cycle; k is the number of samples for the phase leading; k_r is the gain of the RC; $s(z)$ is the LPF, which blocks high-frequency components in the error; and $C(z)$ is the control signal from the RC. The transfer function $G_i(z)$ can be derived from Fig. 5.

$$G_i(z) = k_p + \frac{k_r s(z) z^{-(N-k)}}{1 - q(z) z^{-N}} \tag{7}$$

Substituting Eq. (7) into Eq. (6) yields

$$\frac{E(z)}{i_L^*(z)[1 + G_L(z)G_g(z)D(z)] + G_L(z)D(z)u_g(z)} = \frac{1 - q(z)z^{-N}}{1 + k_p G_d(z)G_L(z) + G_L(z)G_g(z)D(z)} \bullet \frac{1}{1 - z^{-N}R(z)}, \tag{8}$$

where

$$R(z) = q(z) - \frac{k_r s(z) z^k G_d(z) G_L(z)}{1 + k_p G_d(z) G_L(z) + G_L(z) G_g(z) D(z)}.$$

The transfer block diagram of the system error in Eq. (8) is presented in Fig. 6, which consists of five transfer functions: $T_1(z)$, $T_2(z)$, $T_3(z)$, $T_4(z)$, and $T_5(z)$. The five units should be stable to ensure the stability of the entire system. From the

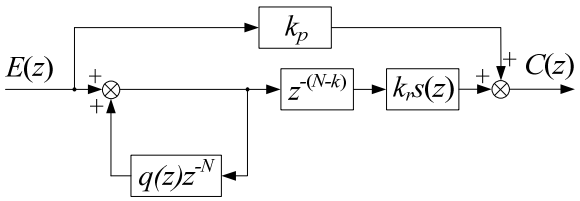

Fig. 5. Structure of the RC paralleled with proportional gain.

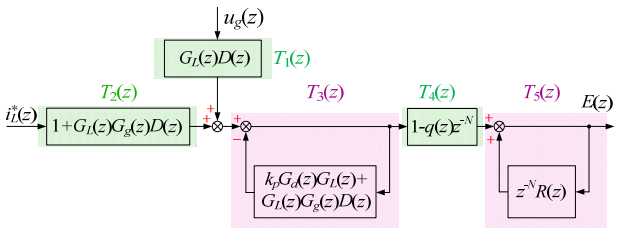

Fig. 6. Transfer block diagram of the system error.

above analysis, all of the poles of $G_L(s)$, $G_g(s)$, and $D(s)$ are located in the left half plane. Therefore, $T_1(z)$ and $T_2(z)$ are stable. The stability of $T_4(z)$ can be guaranteed by selecting a stable $q(z)$, which is easily realized. Thus, the stability of the entire system is only determined by $T_3(z)$ and $T_5(z)$.

$T_3(z)$ is the closed-loop transfer function without the RC, which is a negative feedback unit. Placing the roots of $1+k_pG_d(z)G_L(z)+G_L(z)G_g(z)D(z)=0$ inside the unit circle stabilizes $T_3(z)$. $T_5(z)$ contains a positive feedback loop, and its order is often remarkably high. Therefore, analyzing the stability of this function using a necessary and sufficient criterion, such as pole maps, is relatively complex. A sufficient condition for its stability can be obtained using the small-gain theorem to simplify the analysis process, as shown as follows [30]:

$$|R(z)|<1 \quad \text{for all} \quad z = e^{j\omega T_s}, \quad \omega \in [0, \pi / T_s]. \tag{9}$$

Thus, the closed-loop pole maps and Eq. (9) are used in this study to analyze the robust stability of $T_3(z)$ and $T_5(z)$ as grid impedance varies, respectively. Table I lists the main parameters of the converter system used in the following systematic study. The cutoff frequency and quality factor of the LPF used for voltage filtering are 2 kHz and 0.707, respectively. The LPF $s(z)$ used in the RC has the same form as the LPF used for voltage filtering, as shown in Eq. (5).

The parameters in Table I indicates that k_p=1.5 is selected to set the crossover frequency to approximately one-tenth of the switching frequency [31]. The parameters of the RC are selected as follows: $q(z)$=0.97, k_r=0.7, and k=4, using the design method in [30], and the ω_c and Q of $s(z)$ are 2 kHz and 0.707, respectively. Given the 9.6 kHz sampling and switching frequency, the number of samples in one fundamental cycle N is 192.

In the following analysis, the converter's robust stability is examined with L_g varying up to 0.7 mH, which corresponds to a typical SCR of 10. For z-domain analysis, the bilinear

TABLE I
RATED PARAMETERS OF THE *L*-FILTERED GRID-CONNECTED CONVERTER

Symbol	Description	Value
U_g	Grid voltage (rms)	380 V
I_o	Rated current	100 A
f_s	Switching frequency	9.6 kHz
L	Filter inductance	0.25 mH
R_L	*L*-filter resistor	10 mΩ
C	DC capacitor	2820 μF

transform method (also called the Tustin's method), which is commonly used in engineering application, is used to transform the *s*-domain transfer functions to *z*-domain. Thereafter, the characteristic equation of $T_3(z)$ with the parameter L_g can be derived.

$$\begin{cases} a_1 z^4 + a_2 z^3 + a_3 z^2 + a_4 z + a_5 = 0 \\ a_1 = 37916.12 L_g + 8.59 \\ a_2 = -(66994.57 L_g + 12.85) \\ a_3 = 28460.2 L_g + 10.73 \\ a_4 = -(7601.17 L_g + 4.13) \\ a_5 = 8219.42 L_g + 1 \end{cases} \tag{10}$$

$R(z)$ can also be derived using the *z*-domain transfer functions of each unit. Given these results, the impact of the inductive grid impedance (i.e., SCR) on system stability can be analyzed, as shown in Fig. 7. In Fig. 7(a), $T_3(z)$ has four moving poles as SCR varies down to 10; poles p_1 and p_2 in the *z*-plane move from the right half plane to the left. These left-half-plane poles will cause the high-frequency oscillations in the transient process. Meanwhile, poles p_3 and p_4 move toward the boundary of the unit circle. However, all of the poles are always located inside the unit circle. Thus, $T_3(z)$ is stable when SCR is higher than 10. In Fig. 7(b), the trajectories for the roots of $R(z)$ move toward the boundary of the unit circle rapidly as SCR decreases; this phenomenon indicates poor robust stability of $T_5(z)$ against grid impedance variations. Part of the trajectories will locate outside the unit circle, especially when the SCR is less than 15, and the system may enter the unstable region. Thus, the requirement described in [9] cannot be satisfied.

IV. BPF-BASED GRID VOLTAGE FEEDFORWARD AND ITS ROBUST STABILITY ANALYSIS

The above analysis shows that for the conventional voltage feedforward control, the converter's robust stability is poor when the inductive grid impedance varies. The analyses in Section II indicate that this effect is due to the interaction between the feedforward voltage and the grid-side current through the delay unit. The delay has a low-pass characteristic, and this delay will introduce phase lags, which have a negative

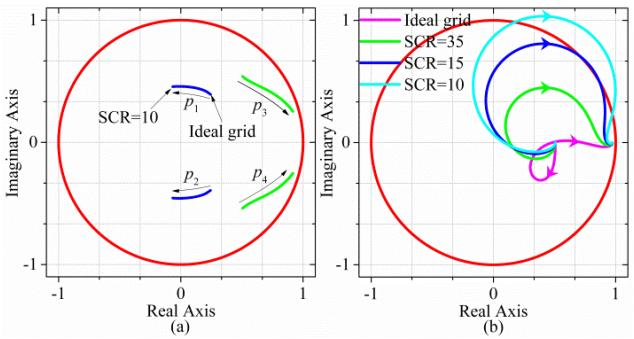

Fig. 7. SCR effect on system stability with the conventional voltage feedforward control. (a) Closed-loop pole maps of $T_3(z)$ with decreasing SCR. (b) Trajectories for the roots of $R(z)$ with different SCRs.

effect on system stability. The phase lags caused by the delay are slightly small at the fundamental frequency (50Hz in this study), and the system's stability is mainly caused by the serious phase lags at relatively higher frequencies. If the magnitudes at the high frequencies are lowered, then gain stabilization can be realized despite the serious phase lags; thus, the converter's robust stability can be improved [32]. Given that the converter's startup performance is mainly affected by the fundamental grid voltage feedforward, the BPF is adopted in this study to be incorporated in the feedforward path to modify the magnitudes of the high-frequency components, except for the fundamental grid voltage, and offer gain stabilization. The BPF model can be expressed in the *s*-domain as

$$G_{BPF}(s) = \frac{\Delta\omega s}{s^2 + \Delta\omega s + \omega_0^2}, \tag{11}$$

where $\Delta\omega$ and ω_0 are the bandwidth and the center frequency of the BPF, respectively. In this study, ω_0 is selected as 100 π (rad/s) to extract the fundamental grid voltage. The bilinear transform is also used to obtain $G_{BPF}(z)$ with $\Delta\omega$=942 (rad/s) for the analysis of the converter's robust stability with the BPF-based feedforward method. Afterward, by replacing the $G_F(z)$ included in $T_3(z)$ with the $G_{BPF}(z)$, the characteristic equation of $T_3(z)$ with the parameter L_g can be derived as

$$\begin{cases} a_1 z^4 + a_2 z^3 + a_3 z^2 + a_4 z + a_5 = 0 \\ a_1 = 8697.6 L_g + 2.02 \\ a_2 = -(27243.36 L_g + 5.9) \\ a_3 = 29560.3 L_g + 6.83 \\ a_4 = -(12173.89 L_g + 3.95) \\ a_5 = 1159.35 L_g + 1 \end{cases} . \tag{12}$$

The $R(z)$ for the proposed BPF-based feedforward method can also be obtained by replacing $G_F(z)$ with $G_{BPF}(z)$. Figure 8 shows the closed-loop pole maps of $T_3(z)$ and the trajectories for the roots of the $R(z)$ as SCR varies down to three. In Fig. 8(a), all of the poles of $T_3(z)$ move inside the unit circle when SCR>3, which indicates the stability of $T_3(z)$ for the proposed method. Furthermore, Fig. 8(b) shows that the trajectories for

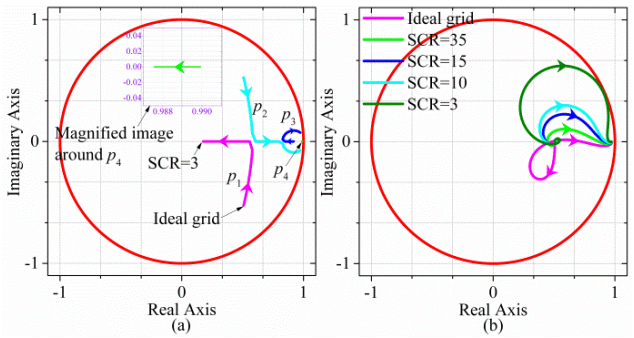

Fig. 8. SCR effect on system stability with the BPF-based voltage feedforward control. (a) Closed-loop pole maps of $T_3(z)$ with decreasing SCR. (b) Trajectories for the roots of $R(z)$ with different SCRs.

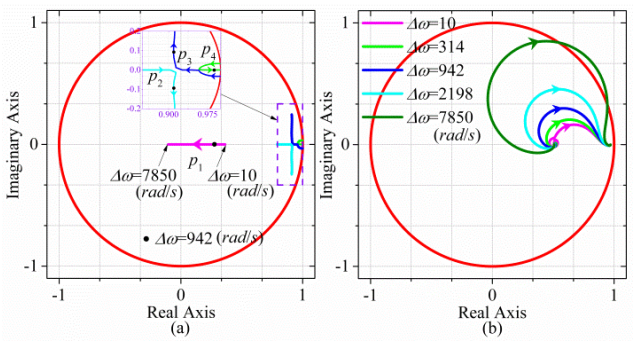

Fig. 9. Effect of the BPF's bandwidth on system stability for the BPF-based voltage feedforward control under SCR=10. (a) Closed-loop pole maps of $T_3(z)$ with increasing bandwidth. (b) Trajectories for the roots of $R(z)$ with different bandwidths.

the roots of $R(z)$ move toward the boundary of the unit circle remarkably slowly as the SCR decreases, indicating strong robust stability of $T_5(z)$ against grid impedance variations. The trajectories are still located inside the unit circle, and the converter can operate stably, especially when SCR=3. Therefore, the converter's robust stability against grid impedance variations is improved obviously.

Selecting the BPF's bandwidth for the proposed BPF-based voltage feedforward control is crucial, because this bandwidth has a significant effect on the converter's robust stability and the transient response during the grid voltage sag. For example, in SCR=10, the characteristic equation of $T_3(z)$ with the parameter $\Delta\omega$ is derived and given in the following for a concrete analysis of this impact.

$$\begin{cases} a_1 z^4 + a_2 z^3 + a_3 z^2 + a_4 z + a_5 = 0 \\ a_1 = -(10.06\Delta\omega + 167998.18) \\ a_2 = 17.94\Delta\omega + 529365.38 \\ a_3 = \Delta\omega - 603051.32 \\ a_4 = -17.94\Delta\omega + 289822.51 \\ a_5 = 9.06\Delta\omega - 48162.6 \end{cases} . \tag{13}$$

In Eq. (13), the closed-loop pole maps of $T_3(z)$ as the bandwidth varies up to 7850 (rad/s) are depicted in Fig. 9(a). The figure indicates that p_1 moves from the right half plane to the left as the bandwidth increases, which will cause the high-frequency oscillations. However, $T_3(z)$ is stable for all $\Delta\omega \in [10, 7850]$. In addition, the trajectories for the roots of $R(z)$ with different values of $\Delta\omega$ are shown in Fig. 9(b), which shows that the trajectories for the roots of $R(z)$ gradually move toward the boundary of the unit circle as $\Delta\omega$ increases. When $\Delta\omega$ increases to 7850 (rad/s), the system may enter the unstable region. Therefore, a smaller the bandwidth means a higher converter's robust stability for the BPF-based voltage feedforward control. However, a smaller bandwidth will slow down the dynamic response to the grid voltage sag. Thus, both the response speed to the grid voltage sag and the robust stability against grid impedance variations should be considered in selecting a proper bandwidth. In practical design, system stability should be considered first; thus the response speed to the grid voltage sag should be compromised by the robust stability requirement. Specifically, the maximum bandwidth of the BPF should ensure the stable operation requirement of the converter under the smallest SCR, such as 10, which is recommended in [9]. In Fig. 9(b), the system has adequate stability margins with SCR=10 with $\Delta\omega$=942 (rad/s).

V. Simulation and Experimental Results

In this section, the simulation and experimental results are presented to verify the analysis and the effectiveness of the proposed voltage feedforward strategy in this study. The key parameters provided in Table I and the parameters of the controller, which were designed above are used in the following simulation study, and these parameters are the same as those used in the experiment.

The system introduced in Fig. 1 is simulated using the PLECS software, and the control algorithms are realized in the embedded dynamic link library. The prototype of the L-filtered grid-connected converter used for the experimental study is shown in Fig. 10, where the TMS320F28335 controller is used for realizing the control algorithm.

Moreover, Fig. 11 presents the simulation and experimental results when the conventional voltage feedforward control is adopted under the ideal grid condition, in which the converter can work stably. However, Fig. 12 shows that severe oscillation arises in the grid-side current when SCR=14. This condition indicates instability and confirms the theoretical expectation in Section III.

For comparison, Figs. 13 and 14 provide the simulation and experimental results for the BPF-based voltage feedforward control strategy under different grid impedance conditions. These results show that the converter can still work stably under the full-load condition when the SCR decreases to 10, which also confirm the theoretical expectation in Section IV. Therefore, the converter's robust stability is obviously improved.

Fig. 10. Experimental prototype of the *L*-filtered grid-connected converter.

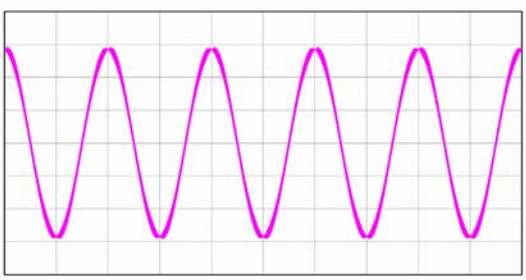

(a) Simulation result.

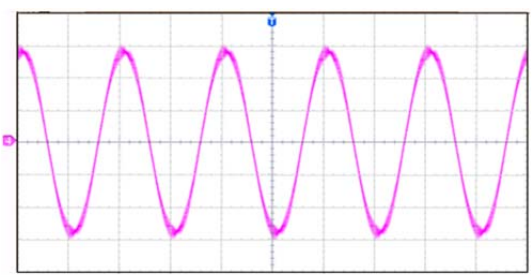

(b) Experimental result.

Fig. 11. Output current waveforms of the converter for the conventional voltage feedforward control strategy under the ideal grid. (x-axis:10 ms/div., y-axis:50 A/div).

In Fig. 15, when SCR=10, the oscillations in the grid-side current appear when the BPF's bandwidth is set to 7850 (rad/s), and the system becomes unstable. Therefore, the theoretical expectations in Section IV are fully confirmed. Thus, for the proposed voltage feedforward method, the BPF's bandwidth should be selected carefully by considering the tradeoff between the response speed to the voltage sag and the system's robust stability.

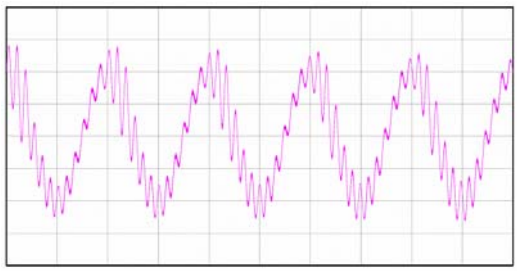

(a) Simulation result.

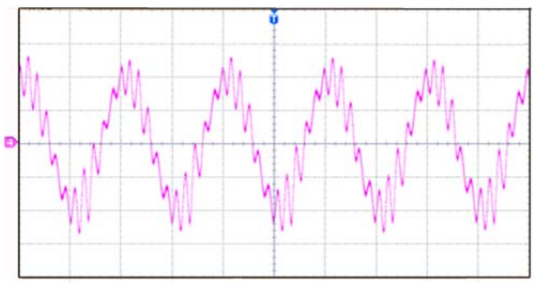

(b) Experimental result.

Fig. 12. Output current waveforms of the converter for the conventional voltage feedforward control strategy with SCR=14. (x-axis:10 ms/div., y-axis:50 A/div).

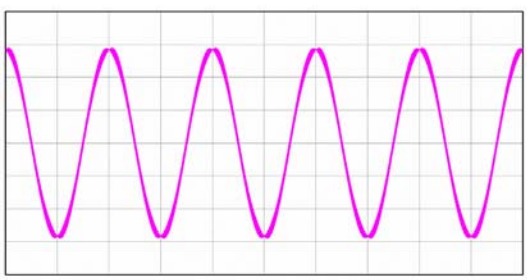

(a) Simulation result.

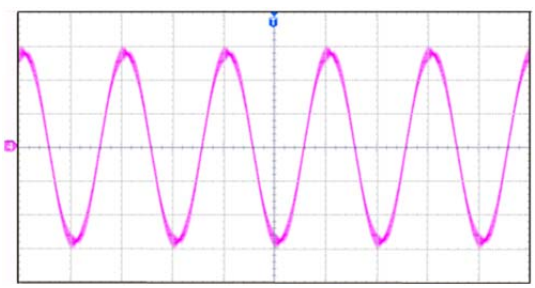

(b) Experimental result.

Fig. 13. Output current waveforms of the converter for the BPF-based voltage feedforward strategy under the ideal grid with $\Delta\omega$=942 rad/s. (x-axis:10 ms/div., y-axis:50 A/div).

All these experimental results closely match with the simulated ones; both results confirm the theoretical expectations and the effectiveness of the proposed BPF-based voltage feedforward strategy. Thus, when the conventional voltage feedforward control is used, the converter can only work stably with SCR>15; this value cannot meet the requirement of [9]. However, with the BPF-based feedforward method, the grid-connected converter can work stably with SCR=10, which can ensure that the grid-connected converter

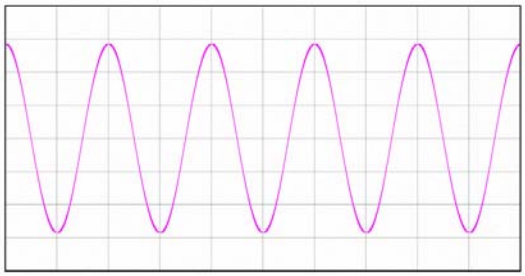

(a) Simulation result.

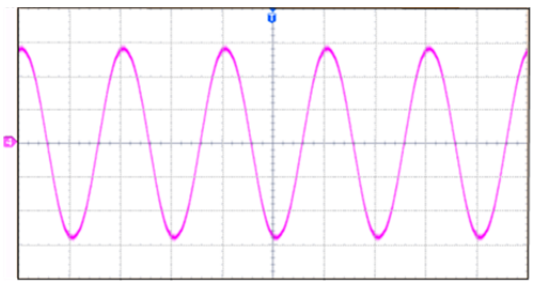

(b) Experimental result.

Fig. 14. Output current waveforms of the converter for the BPF-based voltage feedforward control with SCR=10 and $\Delta\omega$=942 rad/s. (x-axis:10 ms/div., y-axis:50 A/div).

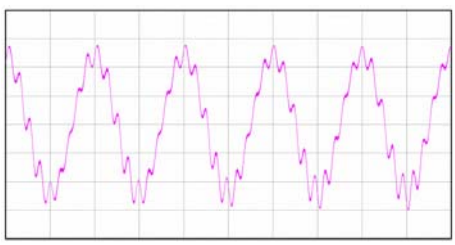

(a) Simulation result.

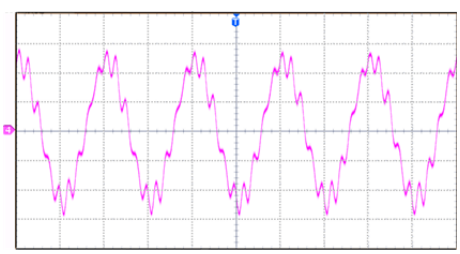

(b) Experimental result.

Fig. 15. Output current waveforms of the converter for the BPF-based voltage feedforward control strategy with SCR=10 and $\Delta\omega$=7850 rad/s. (x-axis:10 ms/div., y-axis:50 A/div)

will meet the standards of [9]; therefore, the converter's robust stability against grid impedance variations is significantly improved. The BPF-based feedforward method is verified by the *L*-filtered converter in this study and is also suitable for the *LCL*-filtered converter.

VI. Conclusions

This study analyzes the root cause of the effect of the grid voltage feedforward on the control system of the *L*-filtered grid-connected converter. Given the poor robust stability of the converter with the conventional voltage feedforward method, a BPF-based voltage feedforward method is proposed to improve the converter's robust stability against grid impedance variations. From the above theoretical analysis, simulation, and experimental results, the following conclusions can be drawn:

1) When the grid voltage feedforward control is used, the converter's stability margins will be largely reduced as the inductive grid impedance increases, and the delay produced by the digital control is the root cause of this effect.
2) The converter's robust stability against grid impedance variations can be remarkably improved by incorporating a BPF in the feedforward path and setting its center frequency as the fundamental frequency.
3) For the BPF-based voltage feedforward strategy, the BPF's bandwidth has a significant effect on the converter's robust stability. Specifically, a smaller bandwidth results in higher converter's robust stability. Therefore, the BPF's bandwidth should be selected by considering the tradeoff between the response speed to the voltage sag and the requirement of the stable operation of the converter under the smallest SCR (i.e., the largest inductive grid impedance).

Acknowledgment

This work was supported by the National Nature Science Foundation of China (51677151, 51507139), Major Scientific and Technological Innovation Projects of Shaanxi Province (2015ZKC02-01), and the Key Discipline Special Foundation of Shaanxi Province (5X1301).

References

[1] A. Alexander and M. Thathan, "Modelling and analysis of modular multilevel converter for solar photovoltaic applications to improve power quality," *IET Renew. Power Gener.*, Vol. 9, No. 1, pp. 78-88, Jan. 2015.
[2] M. Zabaleta, E. Burguete, D. Madariaga, I. Zubimendi, M. Zubiaga, and I. Larrazabal, "LCL grid filter design of a multimegawatt medium-voltage converter for offshore wind turbine using SHEPWM modulation," *IEEE Trans. Power Electron.*, Vol. 31, No. 3, pp. 1993-2001, Mar. 2016.
[3] K. Yang, Y. Wang, and G. Chen, "Design and research on high-reliability HPEBB used in cascaded DSTATCOM," *Journal of Power Electronics*, Vol. 15, No. 3, pp. 830-840, May. 2015.
[4] P. Garanayak, and G. Panda, "Harmonic elimination and reactive power compensation with a novel control algorithm based active power filter," *Journal of Power Electronics*, Vol. 15, No. 6, pp.1619-1627, Nov. 2015.
[5] M. Liserre, R. Teodorescu, and F. Blaabjerg, "Stability of photovoltaic and wind turbine grid-connected inverters for a large set of grid impedance values," *IEEE Trans. Power Electron.*, Vol. 21, No. 1, pp. 263-272, Jan. 2006.
[6] E. M. Lightner, and S. E. Widergren, "An orderly transition to a transformed electricity systems," *IEEE Trans. Smart Grid.*, Vol. 1, No. 1, pp. 3-10, Jun. 2010.

[7] J. Sun, "Impedance-based stability criterion for grid-connected inverters," *IEEE Trans. Power Electron*., Vol. 26, No. 11, pp. 3075-3078, Nov. 2011.
[8] *IEEE standard for interconnecting distributed resources with electric power systems*, IEEE Std 1547-2003, 2003.
[9] *Technical rule for photovoltaic power station connected to power grid*, Q/GDW617–2011, 2011.
[10] Y. Han, P. Shen, and J. M. Guerrero, "Stationary frame current control evaluations for three-phase grid-connected inverters with PVR-based active damped LCL filters," *Journal of Power Electronics*, Vol. 16, No. 1, pp. 297-309, Jan. 2016.
[11] W. Wu, Y. He, and F. Blaabjerg, "An LLCL power filter for single-phase grid-tied inverter," *IEEE Trans. Power Electron*., Vol. 27, No. 2, pp. 782-789, Feb. 2012.
[12] J. Xu, J. Yang, J. Ye, Z. Zhang, and A. Shen, "An LTCL filter for three-phase grid-connected converters," *IEEE Trans. Power Electron*., Vol. 29, No. 8, pp. 4322-4338, Aug. 2014.
[13] J. L. Agorreta, M. Borrega, J. L´opez, and L. Marroyo, "Modeling and control of N-paralleled grid-connected inverters with LCL filter coupled due to grid impedance in PV plants," *IEEE Trans. Power Electron*., Vol. 26, No. 3, pp. 770-785, Mar. 2011.
[14] J.J Sun, W. Hu, H. Zhou, Y.M. Jiang, and X.M. Zha, "A resonant characteristics analysis and suppression strategy for multiple parallel grid-connected inverters with LCL filter," *Journal of Power Electronics*, Vol. 16, No. 4, pp. 1483-1493, Jul. 2016.
[15] M. Liserre, F. Blaabjerg, and R. Teodorescu, "Grid impedance estimation via excitation of LCL-filter resonance," *IEEE Trans. Ind. Appl*., Vol. 43, No. 5, pp. 1401-1407, Sep. 2007.
[16] P. Alemi, S. Y. Jeong, and D.-C. Lee, "Active damping of LLCL filters using PR control for grid-connected three-level T-type converters," *Journal of Power Electronics*, Vol. 15, No. 3, pp. 786-795, May. 2015.
[17] X. Zhou, J. Fan, and A. Q. Huang, "High-frequency resonance mitigation for plug-in hybrid electric vehicles' integration with a wide range of grid conditions," *IEEE Trans. Power Electron*., Vol. 27, No. 11, pp. 4459-4471, Nov. 2012.
[18] Z. Wan, J. Xiong, J. Lei, C. Chen, and K. Zhang, "A modified capacitor current feedback active damping approach for grid connected converters with an LCL filter," *Journal of Power Electronics*, Vol. 15, No. 5, pp. 1286-1294, Sep. 2015.
[19] D. Pan, X. Ruan, C. Bao, W. Li, and X. Wang, "Optimized controller design for LCL-type grid-connected inverter to achieve high robustness against grid-impedance variation," *IEEE Trans. Power Electron*., Vol. 62, No. 3, pp. 1537-1547, Mar. 2015.
[20] X. Wang, F. Blaabjerg, M. Liserre, Z. Chen, J. He, and Y. Li, "An active damper for stabilizing power-electronics-based AC systems," *IEEE Trans. Power Electron*., Vol. 29, No. 7, pp. 3318-3329, Jul. 2014.
[21] D. Dong, B. Wen, D. Boroyevich, P. Mattavelli, and Y. Xue, "Analysis of phase-locked loop low-frequency stability in three-phase grid-connected power converters considering impedance interactions," *IEEE Trans. Ind. Electron*., Vol. 62, No. 1, pp. 310-321, Jan. 2015.
[22] B. Wen, D. Boroyevich, R. Burgos, P. Mattavelli, and Z. Shen, "Analysis of D-Q small-signal impedance of grid-tied inverters," *IEEE Trans. Power Electron*., Vol. 31, No. 1, pp. 675-687, Jan. 2016.
[23] J. Zhou, D. Hui, S. Fan, Y. Zhang, and A. M. Gole, "Impact of short-circuit ratio and phase-locked-loop parameters on the small-signal behavior of a VSC-HVDC converter," *IEEE Trans. Power Del*., Vol. 29, No. 5, pp. 2287-2296, Oct. 2014.
[24] L. Zhang, L. Harnefors, and H.-P. Nee, "Power-synchronization control of grid-connected voltage-source converters," *IEEE Trans. Power Syst*., Vol. 25, No. 2, pp. 809-820, May. 2010.
[25] L. Zhang, L. Harnefors, and H.-P. Nee, "Interconnection of two very weak ac systems by VSC-HVDC links using power-synchronization control," *IEEE Trans. Power Syst*., Vol. 26, No. 1, pp. 344-355, Feb. 2011.
[26] S. Zhou, X. Zou, D. Zhu, Y. Kang, L. Tong, and X.Gao, "LCL type grid-connected converter no startup inrush current control method based on capacitor branch voltage feedforward," in *Industrial Electronics Society, IECON 2015-41st Annual Conference of the IEEE*, pp. 1471-1476, Nov. 2015.
[27] J. Xu, S. Xie, and T. Tang, "Evaluations of current control in weak grid case for grid-connected LCL-filtered inverter," *IET Power Electron*., Vol. 6, No. 2, pp. 227-234, Feb. 2013.
[28] J. Xu, S. Xie, and T. Tang, "Improved control strategy with grid-voltage feedforward for LCL-filter-based inverter connected to weak grid," *IET Power Electron*., Vol. 7, No. 10, pp. 2660-2671, Oct. 2014.
[29] T.-F. Wu, K.-H. Sun, C.-L. Kuo, and C.-H. Chang, "Predictive current controlled 5-kW single-phase bidirectional inverter with wide inductance variation for DC-microgrid applications," *IEEE Trans. Power Electron*., Vol. 25, No. 12, pp. 3076-3084, Dec. 2010.
[30] S. Jiang, D. Cao, Y. Li, and F.Z. Peng, "Grid-connected boost-half-bridge photovoltaic microinverter system using repetitive current control and maximum power point tracking," *IEEE Trans. Power Electron*., Vol. 27, No. 11, pp. 4711-4722, Nov. 2012.
[31] R. W. Erickson and D. Maksimovic, *Fundamentals of Power Electronics*, 2nd ed. Norwell, MA: Kluwer, 2001：330-410.
[32] G. F. Franklin, D.J. Powell and A. E. Naeini, *Feedback Control of Dynamic Systems*, 6th ed., Addison-Wesley Professional, Chap. 6.7.6, 2009.

Shude Yang was born in Henan, China in 1986. He received his B.S. and M.S. degrees in Electrical Engineering from Henan Polytechnic University, Jiaozuo, China in 2009 and 2012, respectively. Since 2012, he has been working toward his Ph.D. degree in the School of Automation and Information Engineering, Xi'an University of Technology, Xi'an, China. His current research interests include power quality, renewable energy generation, and the control and stability analysis of grid-connected converter systems.

Xiangqian Tong was born in Shaanxi, China in 1961. He received his B.S. degree in Electrical Engineering from the Shaanxi Institute of Technology, Hanzhong, China in 1983; his M.S. degree from the Xi'an University of Technology, Xi'an, China in 1989; and his Ph.D. degree in Electrical Engineering from Xi'an Jiaotong University, Xi'an, China in 2006. He joined the Xi'an University of

Technology in 1989. Since 2002, he has been a professor and the academic leader of the Electrical Engineering Department at Xi'an University of Technology. His current research interests include the application of power electronics in power systems, and the control of power quality, especially power filters, static synchronous compensators, and high voltage direct current.

Jun Yin was born in Xinjiang Uygur Autonomous Region, China in 1978. He received both his B.S. and M.S. degrees from Xi'an University of Technology, Xi'an, China in 2001 and 2009, respectively. He joined the Xi'an University of Technology in 2001 after receiving his B.S. degree. Currently, he is a lecturer at the university. His current research interests include the application of power electronics in power system and power quality.

Haiyan Wang was born in Gansu, China in 1980. She received her B.S. and M.S. degrees in Electrical Engineering from North China Electric Power University, Baoding, China in 2002 and 2005, respectively. Since 2010, she has been working toward her Ph.D. degree at the School of Automation and Information Engineering, Xi'an University of Technology, Xi'an, China. Her current research interests include microgrid energy management, optimization, and coordination control of microgrids.

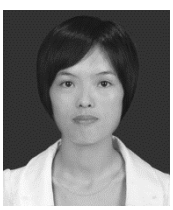

Yaping Deng was born in Shanxi Province, China in 1984. She received her B.S., M.S., and Ph.D. degrees in Electrical Engineering from Xi'an University of Technology, Xi'an, China in 2008, 2011, and 2015, respectively. Her research interests include analysis of power quality and control of hybrid power filter.

Le Liu was born in Shanxi, China in 1993. She received her B.S. degree in Electrical Engineering from the Xi'an University of Technology in 2015. Since 2015, she has been working toward her M.S. degree in the School of Automation and Information Engineering, Xi'an University of Technology. Her current research interests include the modeling and stability analysis of grid-connected converter systems.